P506

Buckling based laser forming process: concave or convex

Wenchuan Li and Y. Lawrence Yao
Department of Mechanical Engineering, Columbia University
New York, NY 10027, USA

Abstract

Concave laser forming can be readily achieved, while convex forming may occur through buckling but the buckling direction heavily depends on the sheet surface and pre-strain condition. A new laser-scanning scheme is postulated, by which convex forming can be effected insensitive to the above mentioned initial conditions. The postulate is successfully validated by experimental and numerical results. The effect of the scanning parameters on the certainty of the convex forming are further investigated experimentally and numerically. The simulation results are in agreement with experimental observations. The numerical simulation model developed is also used to study the transient temperature, stress, and strain-state and provide further insight to the convex forming process.

1. Introduction

There are occasions in practical applications where convex forming is required. Fig. 1 shows an example where concave laser bending can not be applied due to impossible access by the laser beam. It has been shown that convex bending is possible under the buckling mechanism (BM), which is induced when the ratio of laser beam diameter to sheet thickness is large, resulting lower through-thickness temperature gradient. A local elastic buckling and plastic deformation takes place as a result of the thermal expansion which is more or less uniform throughout the sheet thickness (Arnet and Vollertsen, 1995).

But understandably the direction of the buckling heavily depends on the sheet conditions including surface finish and pre-strain. For example, if a sheet is slightly bent, the buckling will most likely take place in the bent direction. In fact, Arnet and Vollertsen (1995) conducted research on convex bending using slightly pre-bent sheets. They experimentally investigated dependency of bend angle on laser power, scanning velocity and beam diameter for steel (St14), AlMg3 and Cu at different values of thickness. They also conducted a well-known experiment, in which unbent but heavily constrained samples were used to demonstrate the existence of the buckling mechanism and the feasibility of convex bending under the condition. The sample is mechanically constrained at both ends instead of clamping on one side only. Holzer, et al. (1994) conducted a numerical simulation under a similar condition. Vollertsen, et al. (1995) proposed an analytical model for laser forming under the buckling mechanism. An expression for the final bending angle was obtained using the elementary theory of bending. The model does not determine the direction of the buckling.

For industrial applications, pre-bending a flat workpiece or to heavily constraining a sheet in order to effect convex bending is not economic for obvious reasons and sometimes impossible as seen in Fig. 1. It is postulated that, under the process condition of buckling, if the starting point of the laser scan is at a point other than one on a sheet edge, the direction of buckling will be certain, that is convex. In almost all laser forming work reported to date, the scan starts from an edge of the sheet. The postulate is based on the fact that although the temperature difference between the top and

bottom surface is small under the buckling mechanism, the flow stress is slightly lower and the tendency of thermal expansion is slightly higher at the top surface because of the slightly higher temperature there (Vollertsen et al., 1995). The slight difference will be amplified by the heavier mechanical constrains introduced by the non-edge starting point which is completely surrounded by material. As the result, the amplified difference is sufficient to lead buckling to take place in the convex direction. Once the buckling occurs in that direction, the rest of the forming process will be in that direction. The postulate is validated by the experimental and numerical results to be explained below.

2. Experiments

Instead of starting laser scanning from an edge (i.e., X_s=0 in Fig. 2), a non-zero value of X_s was used for the reasons stated before. A scan started from a point X_s mm away from the left edge rightward till reaching the right edge. To complete the scan, the scan resumed at a point X_s mm away from the right edge leftward till reaching the left edge. The overlap in scanning was primarily to reduce the so-called edge effect (Bao & Yao, 1999).

The specimen size was 80×80 mm. Two values of thickness, i.e., 0.61 and 0.89 mm were examined. The material was low carbon steel, AISI 1010. The sheet metal was scanned with a PRC1500 CO_2 laser system with the maximum power of 1.5 kW. The power density has a Gaussian distribution (TEM_{00}). The diameter of the laser beam is defined as the diameter at which the power density becomes $1/e^2$ of the maximum power value. To obtain a BM-dominated laser forming process, the ratio of beam diameter to sheet thickness was kept high. The laser power used ranges from 600 to 1,350 W, scanning velocity 18 to 60 mm/s, beam diameter from 12 to 15 mm.

The samples were first cleaned using propanol and then coated with graphite to increase coupling of laser power. During forming, the samples were clamped at one side. A coordinate measuring machine was used to measure the bending angle at different positions along the scanning path. An average bending angle was then calculated based on the measurements of the sample.

3. Theoretical aspects

For an isotropic material, the relationship between stress σ_{ij} and strain ε_{ij} including the influence of temperature can be written in terms of tensor as (Boley and Weiner, 1997)

$$\varepsilon_{ij} = \frac{1}{E}[(1+\gamma)\sigma_{ij} - \gamma\delta_{ij}\sigma_{kk}] + \delta_{ij}\alpha\Delta T \qquad (1)$$

where E is the modulus of elasticity, γ the Poisson's ratio, δ_{ij} the Kronecker delta, α the coefficient of thermal expansion, and ΔT the temperature change. In a BM-dominated laser forming process, the sheet thickness is much smaller than the laser beam size and other dimensions, and the temperature gradient is also small in the thickness direction. Therefore, the stress-state that the sample undergoes can be regarded as in-plane stress-state. The mechanical behavior of the sheet can be described as follows. In the discussion, axis x and y be located in the mid-plane of the sheet.

The membrane forces per unit length for a thin plate can be written in matrix form as (Thornton, et al., 1993)

$$\begin{bmatrix} N_x \\ N_y \\ N_{xy} \end{bmatrix} = \underline{\underline{A}} \begin{bmatrix} \frac{\partial u}{\partial x} \\ \frac{\partial v}{\partial y} \\ \frac{\partial u}{\partial y} + \frac{\partial v}{\partial x} \end{bmatrix} + \underline{\underline{A}} \begin{bmatrix} \frac{1}{2}\left(\frac{\partial w}{\partial x}\right)^2 \\ \frac{1}{2}\left(\frac{\partial w}{\partial y}\right)^2 \\ \frac{\partial w}{\partial x}\frac{\partial w}{\partial y} \end{bmatrix} - \underline{N_T} \tag{2}$$

where

$$\underline{\underline{A}} = \frac{Es}{1-\gamma^2} \begin{bmatrix} 1 & \gamma & 0 \\ \gamma & 1 & 0 \\ 0 & 0 & \frac{1-\gamma}{2} \end{bmatrix}, \quad \underline{N_T} = \frac{E\alpha}{1-\gamma} \int_{-\frac{s}{2}}^{\frac{s}{2}} \begin{bmatrix} \Delta T(x,y,z) \\ \Delta T(x,y,z) \\ 0 \end{bmatrix} dz, \tag{3}$$

N_x, N_y, and N_{xy} are the membrane forces per unit length, $\underline{N}$ is their vector representation, $\underline{\underline{A}}$ is the stiffness matrix, u and v are in-plane displacements of points on the middle surface of the plate, w is the transverse deflection, $\underline{N_T}$ is the membrane force vector induced by a temperature change $\Delta T(x,y,z)$ from an initial temperature, and s the plate thickness. The second term on the right hand side of Eq. (2) is nonlinear strain component corresponding to the transverse deflection. If assuming small transverse deflection, it can be neglected.

The deflections of the buckled plate is obtained by buckling equation (Thornton, et al., 1994)

$$\nabla^4 w = \frac{1}{k}\left(N_x \frac{\partial^2 w}{\partial x^2} + 2N_{xy}\frac{\partial^2 w}{\partial x \partial y} + N_y \frac{\partial^2 w}{\partial y^2} \right) \qquad k = \frac{Es^3}{12(1-\nu^2)} \tag{4}$$

where k is the bending stiffness of the plate and ∇^2 is potential operator $\nabla^2 = \frac{\partial^2}{\partial x^2} + \frac{\partial^2}{\partial y^2}$. N_x, N_y, and N_{xy} can in fact be obtained by multiplying corresponding stresses by the plate thickness, and can be obtained from the Airy's stress function F

$$N_x = \frac{\partial^2 F}{\partial y^2} s, \qquad N_y = \frac{\partial^2 F}{\partial x^2} s, \qquad N_{xy} = -\frac{\partial^2 F}{\partial x \partial y} s \tag{5}$$

The Airy's stress function F satisfies the membrane equation

$$\nabla^4 F = -E\alpha\nabla^2 T \tag{6}$$

where T is the temperature field that the plate is subjected to. Note Eq. (6) is equivalent to Eq.(2) if small transverse deflection is assumed.

To describe the post-buckling problem where the transverse deflection corresponding to the nonlinear term in Eq. (2) is no longer small, the Airy's stress function F has to satisfy the following von Kármán's equation

$$\nabla^4 F = -E\alpha\nabla^2 T + E\left[\left(\frac{\partial^2 w}{\partial x \partial y} \right)^2 - \frac{\partial^2 w}{\partial x^2}\frac{\partial^2 w}{\partial y^2} \right] \tag{7}$$

For plastic thermal buckling of an isotropic homogeneous plate with the in-plane stress state, the buckling equation is (Iyengar, 1988)

$$\left(1-\frac{3}{4}\lambda\frac{N_x^2}{\overline{N}^2}\right)\frac{\partial^4 w}{\partial x^4}+2\left(1-\frac{3}{2}\lambda\frac{N_x N_y}{\overline{N}^2}\right)\frac{\partial^4 w}{\partial x^2\partial^2 y}+\left(1-\frac{3}{4}\lambda\frac{N_y^2}{\overline{N}^2}\right)\frac{\partial^4 w}{\partial y^4}+$$

$$+\frac{N_x}{\overline{D}}\frac{\partial^2 w}{\partial x^2}+\frac{N_y}{\overline{D}}\frac{\partial^2 w}{\partial y^2}+2\frac{N_{xy}}{\overline{D}}\frac{\partial^2 w}{\partial x\partial y}=0 \tag{8}$$

$$\overline{D}=\frac{E_s s^3}{9},\qquad \lambda=1-\frac{E_t}{E_s} \tag{9}$$

where $E_s=\dfrac{\overline{\sigma}}{\overline{\varepsilon}}$ is the secant modulus, $\overline{\sigma}$ the effective stress, $\overline{\varepsilon}$ the effective strain, $\overline{N}=\overline{\sigma}s$, and E_t the tangent modulus. Analytical solutions for the laser forming process are difficult to obtain without significant simplifications. Instead, numerical simulation is conducted.

4. Numerical simulation

The assumptions made for the numerical modeling are as followings. Workpiece materials are isotropic. The rate of deformation is the sum of the elastic strain rate, plastic strain rate, and thermal strain rate. The heating and deformation in the laser forming is symmetrical about the laser-scanning path and the symmetric plane is assumed adiabatic. Heat generated by plastic deformation is negligible because it is small as compared with heat input by laser beam. Therefore a sequential thermal-mechanical analysis will suffice. Laser forming process is so controlled that the maximum temperature in the workpiece is lower than melting temperature of sample material. No cooling of gas or water jet is followed after laser scanning.

The boundary conditions are described follow. Heat flux generated by laser beam is only applied to top surface with a non-uniform distribution. Free heat convection with air occurs on the all surfaces except the symmetric plane: $q = h\,(T - T_0)$, where h is the heat transfer coefficient, and $T_0 = T_0\,(x, t)$ the surrounding temperature. Radiation takes place on the same surfaces: $q = R\,((T - T_Z)^4 - (T_0 - T_Z)^4)$, where R is the radiation constant, and T_Z the absolute zero on the temperature scale used. The initial temperature is set as 300K. On the symmetric plane, no displacement in the Y direction occurs throughout the laser forming process.

The numerical simulation is conducted using code ABAQUS. PCL cluster function is used to create mesh seed along the Y direction so that a wider dense-mesh area than using one way bias can be obtained, which is better for BM-dominated convex laser forming process associated with large beam diameter. The same mesh is created for both thermal and structural analyses. Three-dimensional heat-transfer elements with eight nodes DC3D8 is used for thermal analysis, and continuum stress/displacement elements with the same dimension and number of nodes C3D8 for structure analysis. Two steps corresponding to first and second scans are created in thermal and structural analysis to realize energy input for each scan. After thermal analysis corresponding to heat flux input by laser beam, structure analysis is run to obtain the associated displacements, stresses, and elastic and plastic strains in different directions. This is based on the fact that heat generated by plastic deformation is small as compared with heat input by laser beam and is negligible. Heat flux is determined by the maximum intensity in the center of laser beam with Gaussian distri-

bution (TEM_{00}) and the distance of calculating point from the laser-beam center. That depends on laser beam power, absorption coefficient, beam diameter, scanning velocity, and the distance. A FORTRAN program is developed to define the magnitude of the heat flux generated by laser beam for specific positions on the top surface of the workpiece as a user subroutine. In the model of the finite element analysis, nonlinear analysis is used because of characteristics of the forming process. Von Mises criterion is used as the yield criterion in the simulation. Temperature-dependent work hardening of the material due to plastic deformation is considered. Strain-rate and temperature effects on flow stress are taken into account (Li and Yao, 1999a)

5. Results and discussion

Fig. 3 is a histogram of bending direction for different distance from edge, X_s. At each distance, four samples were laser formed. When X_s=0, i.e., scanning from an edge, the bending direction is uncertain, two samples were bent concavely and two convexly. This is consistent with published results, that is, in a BM-dominated laser forming process, buckling will occur but the direction of the buckling is uncertain and heavily depends on the initial stress/strain state and surface condition. A small disturbance in favor of a particular direction will easily induce the buckling towards that direction. When X_s increases, i.e., the starting point of the scanning moving away from the edge, the bending becomes predominantly convex. When the starting point approaches the middle of the plate, that is, X_s approaches 40 mm, the bending is always convex. This clearly confirms the postulate made earlier, that is, even in a BM-dominated laser forming process temperature/thermal expansion at the top surface is slightly high than that at the bottom surface and a slight convex bending will occur first. This is also the case in TGM-dominated processes or BM-dominated processes with the starting point of scanning at an edge. But the difference is that when the starting point is not at the edge, the initial convex bending will continue (instead of reversing) due to the added mechanical constraints of the surrounding materials. As a result, the rest of the forming process will understandably follow its lead. More discussions will be given later in the paper when transient simulation results are discussed. For the rest of the experiments and all simulation studies, X_s=25 mm.

Shown in Fig. 4 are comparisons between numerical and experimental results of bending angle vs. power and non-dimensional parameter V_n. V_n is defined as $V_s s/\alpha_d$. The physical meaning of V_n is the ratio of through-thickness unheated part of the sheet to thickness. For obvious reasons, the bending angle becomes more negative with laser power increase, and less negative with velocity increase. Fig. 4 shows that the simulation results are fairly consistent with the experimental measurements.

Fig. 5 shows the relationship between bend angle and dimensionless velocity V_n at two different power levels. It is obvious that as V_n increases, the absolute value of bending angle reduces. A threshold value of V_n can be seen, above which, no bending takes place due to insufficient energy input. Shown in Fig. 6(a) is dependence of bend angle on laser power under two different velocities. As seen, the higher the power, the larger the absolute value of the bending angles due to obvious reasons. Shown in Fig. 6 (b) is bending vs. power under two different values of thickness. Again the trends are readily understood. These results are of course different from the condition of constant line energy (Li & Yao, 1999b).

In order to obtain further insights into the reasons that the convex forming is always obtained when the starting point of laser scanning moves from an edge to a point closer to the center of the sheet, the transient plots from simulation are shown in Fig. 7. The plots are for the starting point X_s=25 mm. At time=0 sec, the scan begins at the starting point rightward, proceeds till it passes the right edge, and waits there for quite a few minutes for the sheet to cool down before completing the scan rightward (Fig. 2). Shown in Fig. 7 is time history of the first 100 seconds.

Fig. 7a confirms that, although small, there is a temperature difference between the top and bottom surface under the process condition, which is known to induce the buckling mechanism (BM). As a result, there is slightly more thermal expansion at the top surface than that at the bottom surface, resulting a small negative bending angle (convex bending) as seen from Fig. 7b. The small convex bending angle in turn causes a slightly more compressive stress at the bottom than that at the top as seen from Fig. 7c. This trend continues till about t=0.7 sec. At the point of time, the convex bending angle has grown big enough to make the buckling happen of course in the same direction, which is the convex direction. This is evident in the dramatic increase in the negative bending angle within a fraction of second (from about 0.7 to 1.1 sec as seen from Fig. 7b). As a result, the compressive stress at the top surface also abruptly reverses its sign to become tensile (Fig. 7c).

It should be pointed out that the initial small convex bending angle exists in laser forming under almost any condition. This includes TGM-dominated processes. This also includes BM-dominated processes in which the starting point of the laser scan is from an edge of the workpiece. In the TGM-dominated processes, the small convex bending angle is quickly reversed to a large concave bending angle because the significant shortening at the top-surface caused by significant temperature gradient through the thickness serves as a strong pulling force during cooling. In the BM-dominated processes in which the starting point of the laser scan is from an edge of the workpiece, the initial small convex bending angle may lead to either directions. This is because the mechanical constraints near the edge are less. As a result, the inducing effect of the initial convex bending angle can be easily overturned by other forms of small disturbances, such as the sheet and surface condition or pre-strain condition at the location.

But this is not the case for the conditions used in this paper. Once an initial small convex bending angle is formed, it is very hard, if not impossible, to reverse because of the heavier mechanical constraints surrounding the starting point. As a result, the buckling can only take place in the same direction as the initial direction, that is, convex direction. In addition, due to the heavier constraint in the case of starting at a non-edge location, the initial small convex bending can be up to 50% larger than that when starting at an edge while all other conditions are kept the same. This again makes it more difficult to reverse the initial convex bending. To further illustrate the point, a laser beam momentarily irradiated at X_s=25 mm while both the laser and workpiece were kept stationary. The caused deformation was measured and plotted in Fig. 8. The deformation in the Z-direction at the location was measured as 0.011 mm, which is about 40% larger than that if the irradiation took place at an edge (X_s=0 mm) obviously because of less mechanical constraints to deformation at the edge.

6. Conclusions

Using the postulated scanning scheme, convex forming is realized with high certainty. The postulation is based on the analysis that the added mechanical constraints by moving the starting point

from an edge to the middle will sustain the initial convex deformation, which exists in both concave and convex forming. The postulate is successfully validated by experimental and numerical results. With the method, neither pre-bending nor additional external mechanical constraints are needed in order to effect convex laser forming. The underlying physical phenomena, including temperature, stress, and strain field near the starting point, are investigated to give better understanding of the forming mechanisms and effects of the new scanning schemes.

References

Arnet, H., and Vollertsen, F., 1995, "Extending laser bending for the generation of convex shapes," IMechE Part B: Journal of Engineering Manufacture, Vol.209, pp.433-442.

Bao, J., and Yao, Y. L., "Analysis and Prediction of Edge Effects in Laser Bending," *Proc. 18th Int. Congress on Applications of Lasers and Electro-Optics (ICALEO '99): Conf. on Laser Materials Processing*, San Diego, Nov., 1999, Section C, pp. 186-195.

Boley, B. A. and Weiner, J. H., 1997, "Theory of Thermal Stresses", Dover Publications, Inc., Mineola, New York.

Holzer, S., Arnet, H., and Geiger, M., 1994, "Physical and numerical modeling of the buckling mechanism," Laser Assisted Net Shape Engineering, Proceedings of the LANE'94, Vol.1 pp. 379-386.

Hsiao, Y.-C., Shimizu, H., Firth, L., Maher, W., and Masubuchi, K., 1997, "Finite element modeling of laser forming," Proc. ICALEO '97, Section A, pp. 31-40.

Iyengar, N. G. R., 1988, Structural Stability of columns and plates, Ellis Horwood Limited, England.

Kyrsanidi, An. K., Kermanidis, Th. B., and Pantelakis, Sp. G., 1999, "Numerical and experimental investigation of the laser forming process," Journal of Materials Processing Technology, Vol. 87, pp. 281-290.

Li, W., and Yao, Y. L., 1999a, "Effects of Strain Rate in Laser Forming," *Proc. 18th Int. Congress on Applications of Lasers and Electro-Optics (ICALEO '99): Conf. on Laser Materials Processing*, San Diego, Nov., 1999, Section F, pp. 107-116.

Li, W., and Yao, Y. L., 1999b, "Laser forming with constant line energy," International Journal of Advanced Manufacturing Technology, to appear.

Thornton, E. A., Kolenski, J. D., and Marino, R. P., 1993, "Finite element study of plate buckling induced by spatial temperature gradients," 34th AIAA/ASME/ASCE/AHS/ASC Structures, Structural Dynamics and Materials Conference, La Jolla, CA, pp. 2313-2326.

Thornton, E. A., Coyle, M. F., and McLeod, R. N., 1994, "Experimental study of plate buckling induced by spatial temperature gradients," Journal of Thermal Stresses, Vol. 17, pp. 191-212.

Vollertsen, F., Komel, I., and Kals, R., 1995, "The laser bending of steel foils for microparts by the buckling mechanism- a model," Modeling Simul. Mater. Sci. Eng. Vol.3., pp.107-119.

Meet the Authors

Wenchuan Li is currently a Ph.D. candidate and Y. Lawrence Yao an Associate Professor in the Department of Mechanical Engineering at Columbia University, where Yao also directs the Manufacturing Engineering Program. Yao has a Ph.D. from Univ. of Wisconsin-Madison.

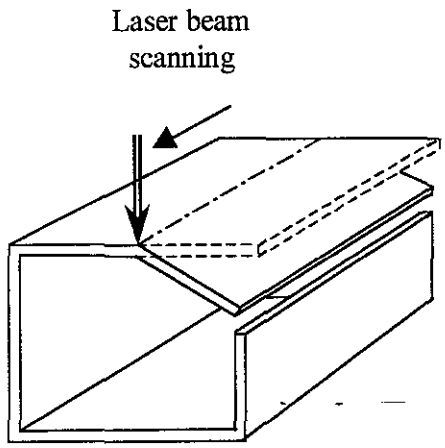

Fig. 1 Example requiring convex forming (dash lines indicating the shape before laser forming)

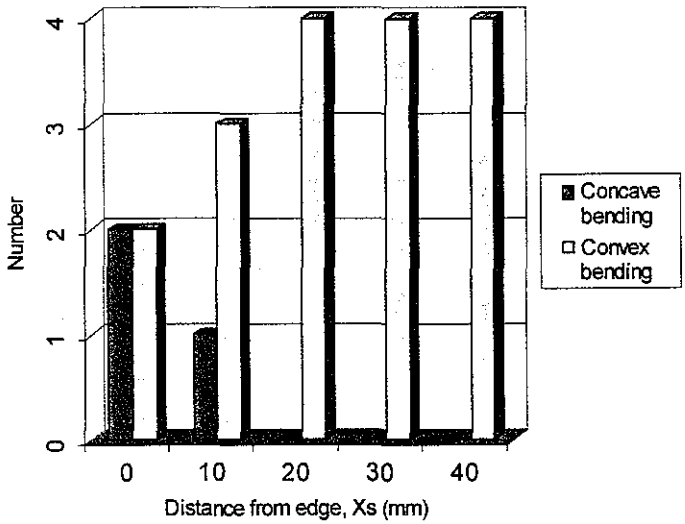

Fig. 3 Histogram of bending direction vs. distance from edge, X_s (power:900W, velocity:30mm/s, beam diameter:14.8mm)

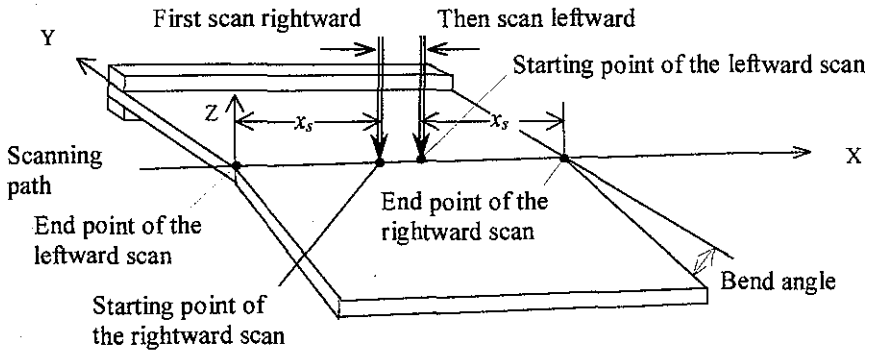

Fig. 2 Scanning scheme for convex laser forming

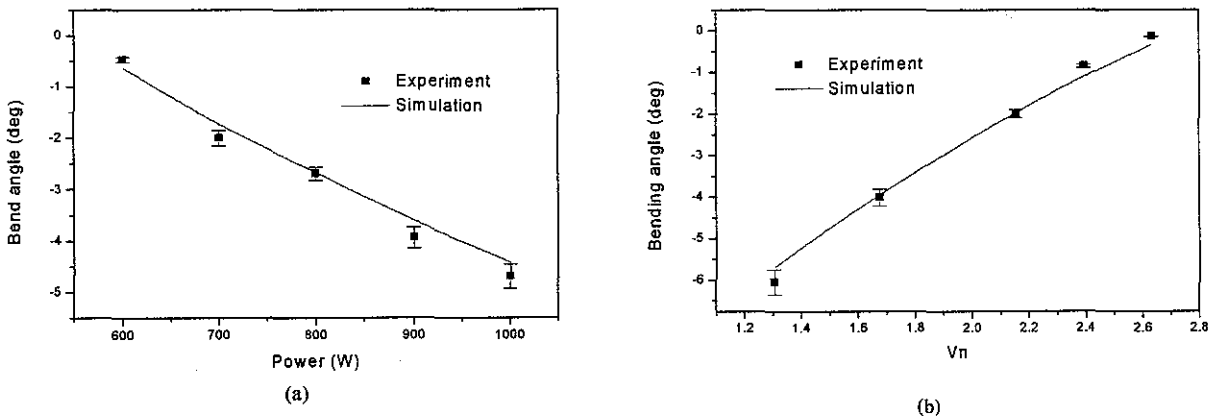

Fig. 4 Numerical and experimental results of variation of bend angle with power p (a, scanning velocity: 30mm/s) and dimensionless velocity v_n (b, power: 700W) (beam diameter: 14.8mm, workpiece size: 80×80×0.89mm)

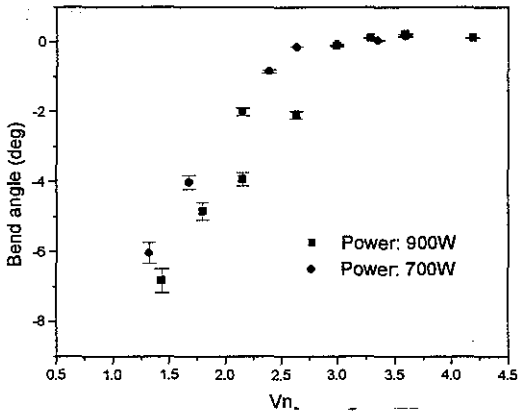

Fig. 5 Bend angle vs. dimensionless velocity v_n (beam diameter: 14.8mm, sample dimension: 80×80×0.89mm)

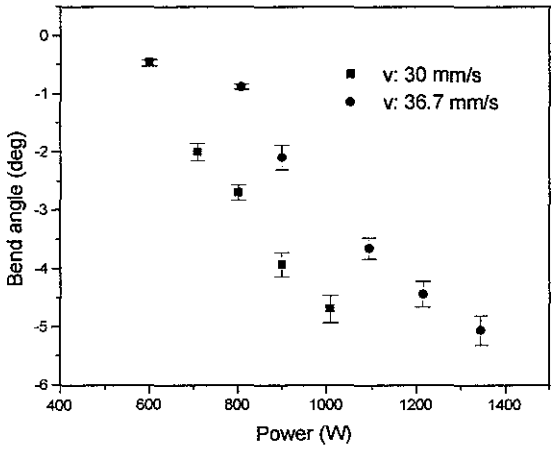

(a)

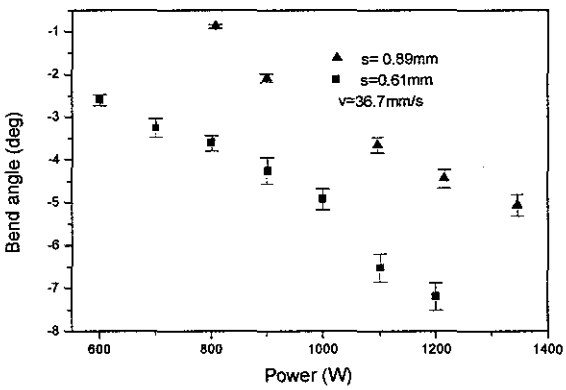

(b)

Fig. 6 Bend angle vs. power (a) at different scanning velocities (sheet thickness: 0.89mm), and (b) at different levels of thickness (both: beam diameter: 14.8mm, sample size: 80×80mm)

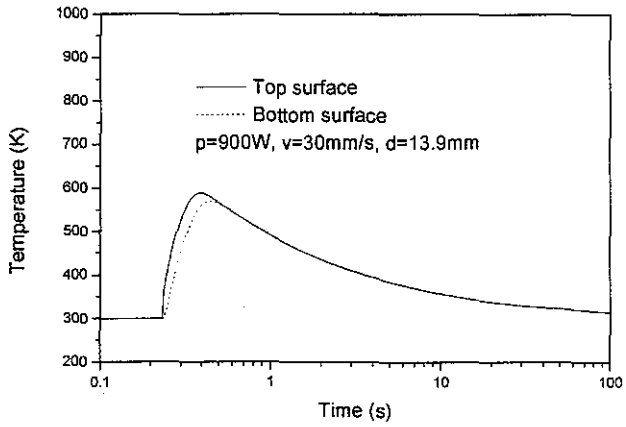

(a)

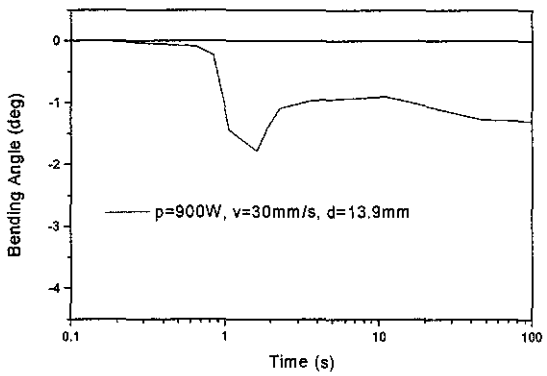

(b)

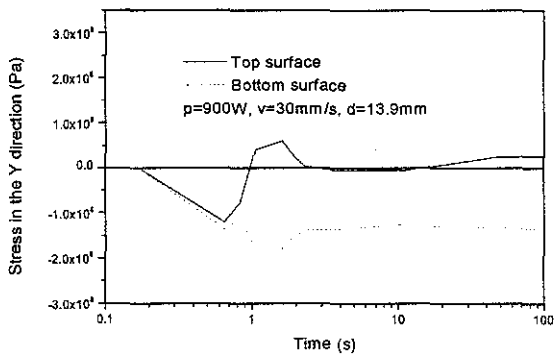

(c)

Fig. 7 Typical time history of (a) temperature, (b) bend angle, and (c) Y-axis stress at the starting point, X_s=25mm (p=900W, v=30mm/s, d=13.9mm, workpiece 80×80×0.89mm)

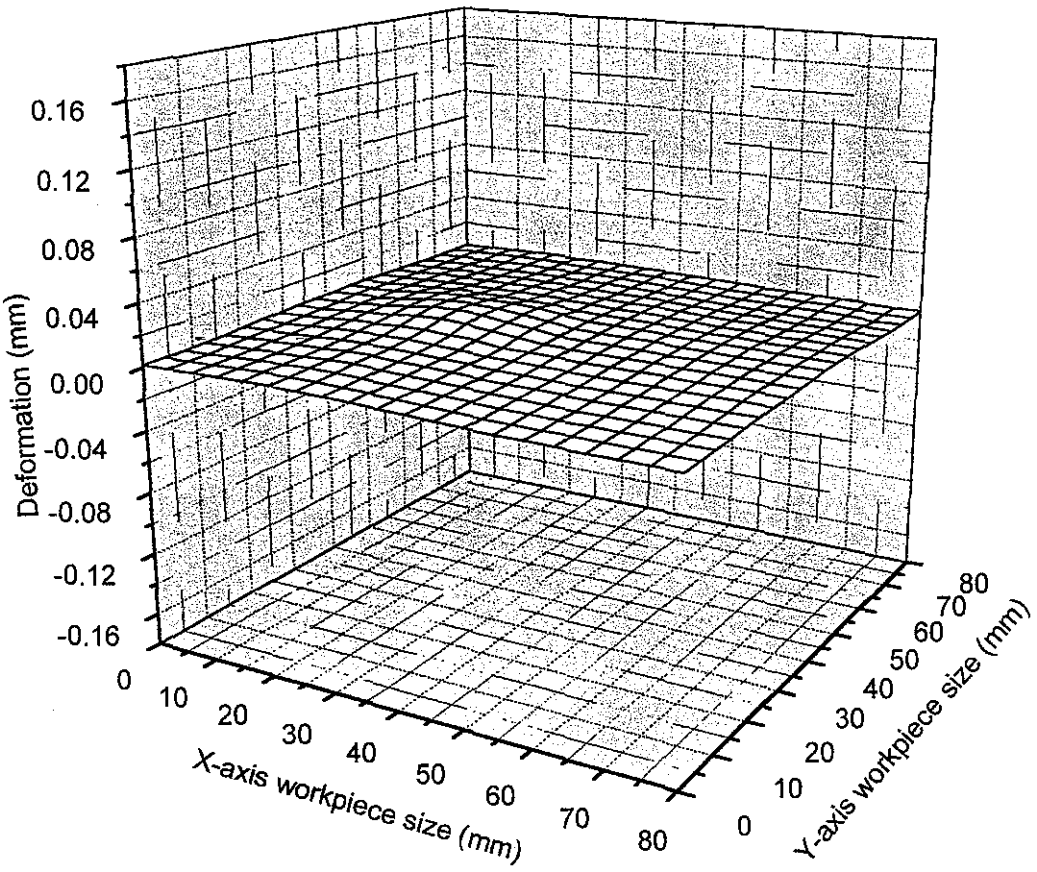

Fig. 8 Deformation at X_s=25 mm caused by laser irradiation (both laser and workpiece stationary, laser duration: 300 ms, beam diameter: 14.8mm, power: 700W, dimension: 80×80×0.89mm)